M. TAKEUCHI[1]
T. TAKANO[1]
S. ICHIHARA[1]
Y. TAKASU[2]
M. KUMAKURA[1,3,4]
T. YABUZAKI[5]
Y. TAKAHASHI[1,4,✉]

Paramagnetic Faraday rotation with spin-polarized ytterbium atoms

[1] Department of Physics, Graduate School of Science, Kyoto University, Kyoto 606-8502, Japan
[2] Department of Electronic Science and Engineering, Graduate School of Engineering, Kyoto University, Kyoto 615-8510, Japan
[3] PREST, JST, 4-1-8 Honcho Kawaguchi, Saitama 332-0012, Japan
[4] CREST, JST, 4-1-8 Honcho Kawaguchi, Saitama 332-0012, Japan
[5] Faculty of Information Science and Arts, Osaka Electro-Communication University, Osaka 572-8530, Japan

ABSTRACT We report the observation of paramagnetic Faraday rotation of spin-polarized ytterbium (Yb) atoms. As the atomic samples, we used an atomic beam, released atoms from a magneto-optical trap (MOT), and trapped atoms in a far-off-resonant trap (FORT). Since Yb is diamagnetic and includes a spin-1/2 isotope, it is an ideal sample for spin physics, such as quantum non-demolition measurement of spin (spin QND), for example. From the results of the rotation angle, we confirmed that the atoms were almost perfectly polarized.

PACS 32.80.Bx; 32.80.Pj; 42.25.Lc

1   Introduction

Faraday rotation is the polarization rotation of linearly-polarized light due to the circular birefringence of the medium. When the refractive index of the medium is $n_\pm$ for circularly polarized light $\sigma_\pm$, respectively, the Faraday rotation angle φ becomes

$$\varphi = \frac{\omega L}{2c}(n_+ - n_-) , \tag{1}$$

where ω is the angular frequency of the probe light, L is the length of the medium, and c is the light velocity (Fig. 1) [1]. In particular, paramagnetic Faraday rotation is a powerful method for probing the spin state of an atomic ensemble [2]. The rotation angle for an atomic ensemble via the paramagnetic Faraday rotation can be written as

$$\varphi = \frac{\alpha t_1}{2} S_z , \tag{2}$$

where α is a real constant, t_1 is the interaction time, and S_z is the total spin component in the probe region parallel to the propagation direction of light [3].

Recently, there has been a renewal of interest in the paramagnetic Faraday rotation for quantum non-demolition measurement of spin (spin QND) [3–5]. Spin QND is not only a quantum measurement, but also has a wide variety of applications. For example, spin squeezing, entanglement of two macroscopic objects, and quantum memory for light have been demonstrated [6–9], and reversible quantum measurement has been proposed [10]. These applications of spin QND will be breakthroughs in not only quantum information processing, but also in precision measurements [11].

The ytterbium (Yb) atoms have many merits for spin QND. (i) Since the electronic ground state of Yb is diamagnetic ($^1S_0$), the magnetic moment has its origin only in nuclear spin, which is three orders of magnitude smaller than the paramagnetic atoms. It is experimentally easier to suppress the fluctuation of the precessions of the spin than that by use of the paramagnetic atom like references [5–9, 12]. Therefore, a longer coherence time will be expected. Moreover, the spin polarization is also easier since the optical pumping process is faster than the Larmor precession. (ii) Yb atoms include a spin-1/2 isotope (^{171}Yb). Since the interaction between spin-1/2 particles and the external electro-magnetic field is described by scalar and vector polarizabilities alone, instead of more general tensor polarizability [2], it can be said that ^{171}Yb is one of the most ideal samples for spin physics. (iii) Yb atoms include also spin-0 isotopes. By comparing the signal from a spin-1/2 isotope with the signals from spin-0 isotopes, calibrations of the experimental system are possible. In Table 1, we summarize the isotopes and the abundance of ytterbium. (iv) Laser-cooling and trapping techniques have already been established [13–16].

As far as we know, however, the observation of the paramagnetic Faraday rotation with spin-polarized Yb atoms has not been reported yet. In this paper, we report the theoretical estimations of the rotation angle, and its observations.

✉ Fax: +81-75-753-3769, E-mail: yitk@scphys.kyoto-u.ac.jp
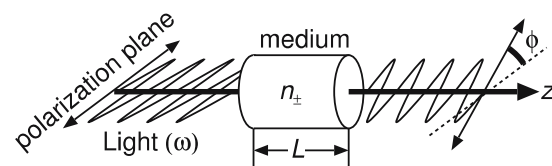
FIGURE 1 Faraday rotation is the polarization rotation of linearly-polarized light due to the circular birefringence of the medium ($n_\pm$). In the case of the paramagnetic Faraday rotation, the rotation angle is proportional to the total spin component parallel to the propagation direction of light (S_z)

Nuclear Spin (I)	Mass Number (M)	Abundance
0	168,170,172,174,176	69.5%
1/2	171	14.3%
5/2	173	16.2%

TABLE 1   Mass number and natural abundance of stable ytterbium categorized by the nuclear spin

As the samples, we used atomic beam, released atoms from a magneto-optical trap (MOT), and trapped atoms in a far-off-resonant-trap (FORT). Simultaneously, we have almost perfectly polarized ^{171}Yb and ^{173}Yb via the optical pumping [2]. From our experimental results, Yb will be considered as one of the best samples for spin QND.

2   Theory

In our experiment, ω is close to the resonance frequency of $^1S_0 \rightarrow {}^1P_1$ transition, ω_0. The electric dipole moment μ_e can be written as [17]

$$\mu_e^2 = \frac{e^2 \sigma_0 \Gamma}{8\pi\alpha_f \omega_0}, \tag{3}$$

where α_f is the fine structure constant, e is the charge of an electron, $\sigma_0 \equiv 6\pi(c/\omega_0)^2$ is the photon-absorption cross section of an atom, and Γ is the natural full linewidth of the transition in angular frequency. In the following calculations, we assume $\omega/\omega_0 \simeq 1$, and that the electric field of light E, or the intensity I is weak,

$$\Omega^2 \equiv \frac{\mu_e^2 E^2}{\hbar^2} = \frac{\Gamma^2 I}{2I_s} \ll (\omega_0 - \omega)^2 + (\Gamma/2)^2, \tag{4}$$

which corresponds to the elimination of the higher-order electric susceptibility. Ω is the Rabi frequency, and I_s is the saturation intensity given by $I_s = \hbar\omega_0 \Gamma/2\sigma_0$ [17]. For Yb, $\omega_0 = 2\pi \times 751.5$ THz, $\Gamma = 2\pi \times 29$ MHz, $\sigma_0 = 7.598 \times 10^{-14}$ m^2, and $I_s = 0.60$ mW/mm^2.

2.1   *Spin-0 isotopes:* ^{168} Yb, ^{170} Yb, ^{172} Yb, ^{174} Yb, ^{176} Yb

In Fig. 2, we depict the level structure and the transition probabilities for $\sigma_\pm$ light of spin-0 isotopes. The refractive indices $n_\pm$ become [18]
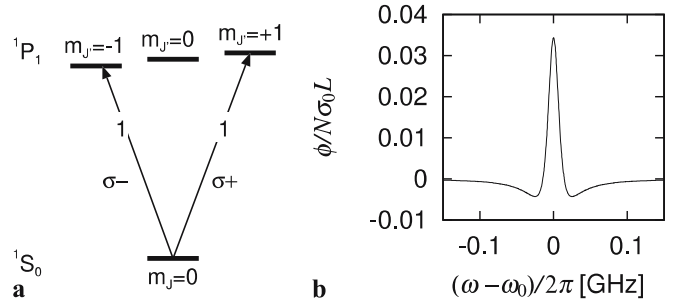
$$n_\pm = 1 + \frac{2\pi\alpha_f c \mu_e^2}{e^2} g_{\pm 1} N \tag{5}$$

where N is the number density of the atoms, $g_{m_{J'}}$ ($m_{J'} = \pm 1$) is given by

$$g_{m_{J'}} = \frac{\omega_{m_{J'}} - \omega}{(\omega_{m_{J'}} - \omega)^2 + (\Gamma/2)^2}, \tag{6}$$

and is the dispersive function of ω at the center frequency $\omega_{m_{J'}}$ which is the resonance frequency between the ground state and the excited state $m_{J'}$. From (5), the rotation angle becomes

$$\varphi = \frac{\Gamma}{8}(g_{+1} - g_{-1})N\sigma_0 L. \tag{7}$$

FIGURE 2   (a) Level structure and the transition probabilities for $\sigma_\pm$ light of spin-0 isotopes. (b) Theoretical calculation of the rotation angle when $\omega_{\pm 1} = \omega_0 \pm 2\pi \times 1$ MHz

It should be noted that the rotation angle is proportional to $N\sigma_0 L$. From (7) it is obvious that the rotation angle vanishes when the excited states are degenerated such as $\omega_{+1} = \omega_{-1}$. This is not the paramagnetic Faraday rotation but the diamagnetic Faraday rotation, and is useful for magnetic field compensation. Since the magnetic moment of $^1P_1$ state is as large as one Bohr magneton, the stray magnetic field parallel to the propagation of light, which leads to the Zeeman splitting of the sublevels $m_{J'} = \pm 1$ in the $^1P_1$ state, can be monitored via this Faraday rotation. In Fig. 2b, we plot (7) as a function of ω. It should be noted that the rotation angle rapidly decreases at off-resonance.

2.2   *Spin-$1/2$ isotope:* ^{171} Yb

To simplify the discussions in the following, we assume that the applied magnetic field is very weak, and so the magnetic sublevels are almost degenerate, and therefore we do not consider the diamagnetic Faraday rotation discussed above. For this isotope, the good quantum number of the $^1P_1$ state is $F' = J' + I$. To derive the transition probabilities of each transition, the additional rule of angular momenta must be considered [19]. The expansion coefficients $\langle J', I; m_{J'}, m_I | J', I; F', m_{F'}\rangle$ can be calculated as

$$|\langle 1, 1/2; \pm 1, \pm 1/2 | 1, 1/2; 3/2, \pm 3/2\rangle|^2 = 1, \tag{8}$$

$$|\langle 1, 1/2; \pm 1, \mp 1/2 | 1, 1/2; 3/2, \pm 1/2\rangle|^2 = \frac{1}{3}, \tag{9}$$

$$|\langle 1, 1/2; \pm 1, \mp 1/2 | 1, 1/2; 1/2, \pm 1/2\rangle|^2 = \frac{2}{3}, \tag{10}$$

and the other coefficients become zero. In Fig. 3, we depict the levels and the probabilities of the each transitions for $\sigma_\pm$ light.

The refractive indices become

$$n_\pm = 1 + \frac{2\pi\alpha_f c \mu_e^2}{e^2}$$
$$\times \left(g^{(3/2)} N_{\pm 1/2} + \frac{2}{3} g^{(1/2)} N_{\mp 1/2} + \frac{1}{3} g^{(3/2)} N_{\mp 1/2} \right), \tag{11}$$

where $g^{(F')}$ is the dispersive function at the center frequency $\omega^{(F')}$, which is the resonance frequency between the ground and each hyperfine excited state F', and $N_{\pm 1/2}$ is the number density of atoms in the ground state $m_I = \pm 1/2$, respectively.
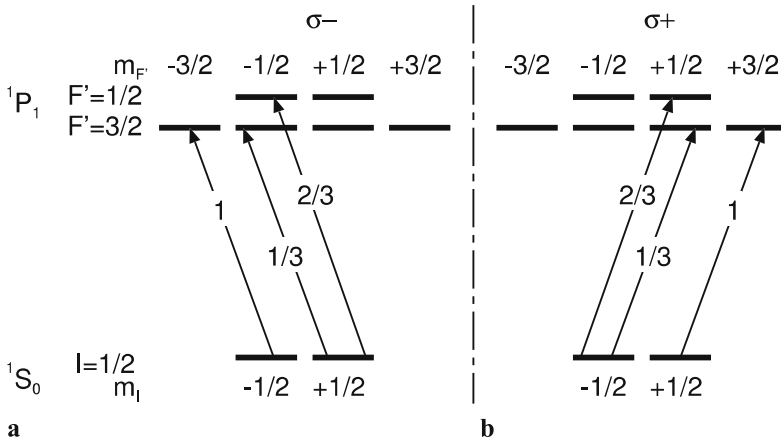
FIGURE 3 Levels and squared transition probabilities of spin-1/2 isotope. (**a**) For σ_- light; (**b**) for σ_+ light

From (11), the rotation angle becomes

$$\varphi = \frac{\Gamma}{12} \left(g^{(3/2)} - g^{(1/2)} \right) p N \sigma_0 L \,, \tag{12}$$

where $p \equiv (N_{+1/2} - N_{-1/2})/N$ is the spin polarization. It is obvious that the rotation angle vanishes when there is no population difference between the ground sublevels such as $p = 0$, and is proportional to $N\sigma_0 L$ as for the diamagnetic Faraday rotation of (7). In Fig. 4, we plot (12) as a function of ω. It should be noted that the rotation angle slowly decreases at off-resonance.

Since the total spin component of an atomic ensemble is written as $S_z = pN\pi w^2 L/2$, that is, p is proportional to S_z, it can be said that from (12) the rotation angle φ always reflects S_z for any detuning, where w is the beam waist of the probe light. In the case of the atoms having complicated level structures, (2) is only s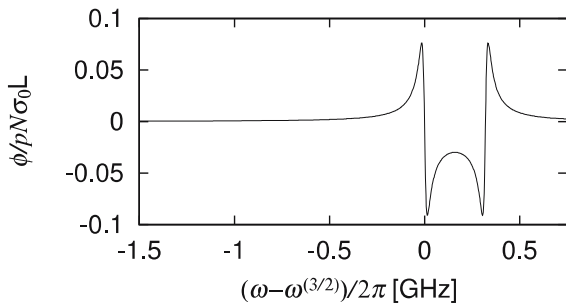atisfied for large detunings [12]. The coupling constant αt_1 decreases, however, for large detunings. This is one of the reasons why the spin-1/2 isotope is the most ideal sample for spin QND.

2.3 *Spin-5/2 isotope:* ^{173}Yb

The level structure of spin-5/2 isotope is complicated as is shown in Fig. 5. To simplify the discussion, we consider the case that the atom is polarized at $m_I = +5/2$ state in the ground state. From the transition probabilities, the rotation angle becomes
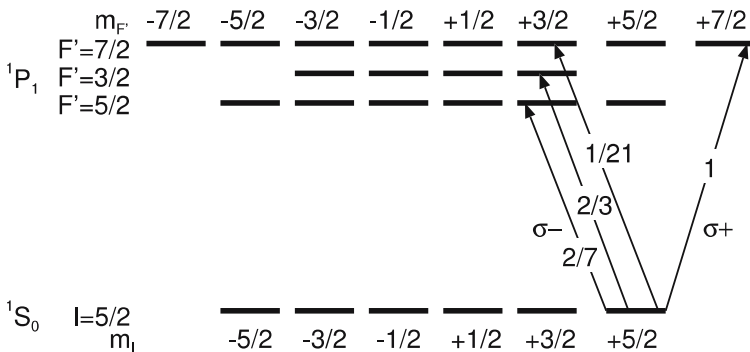
$$\varphi = \frac{\Gamma}{84} \left(10 g^{(7/2)} - 7 g^{(3/2)} - 6 g^{(5/2)} \right) N \sigma_0 L \,, \tag{13}$$

where N is the number density of the atom. In Fig. 6, we plot (13) as a function of ω. It should be noted that the rotation angle vanishes when there is no population difference among the ground sublevels, similar to the case of spin-1/2 isotope.

2.4 *Spin polarization*

As is mentioned above, the rotation angle has non-vanishing value when there is some population difference among the ground sublevels. To make the population difference in the ground states, we performed the optical pumping by using the $^1S_0 \rightarrow {}^1P_1(F' = I)$ transition with circularly polarized light. In Fig. 7, we describe the schematic of the optical pumping with σ_+ light. The atom in $m_I \neq +I$ state absorb σ_+ light, then emit $\sigma_\pm$ or π light and fall to a lower state. By repeating the absorptions and the emissions, all populations fi-

FIGURE 4 Rotation angle of spin-1/2 isotope. Here, we used the value of the hyperfine splitting, $\omega^{(1/2)} - \omega^{(3/2)} = 2\pi \times 320$ MHz [20]
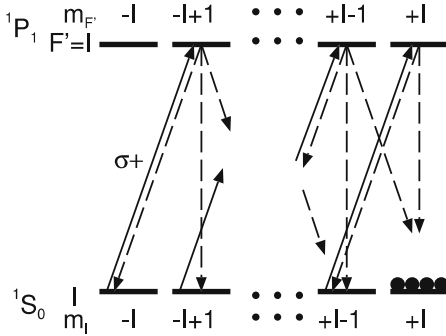

FIGURE 5 Levels and some squared transition probabilities for spin-5/2 isotope
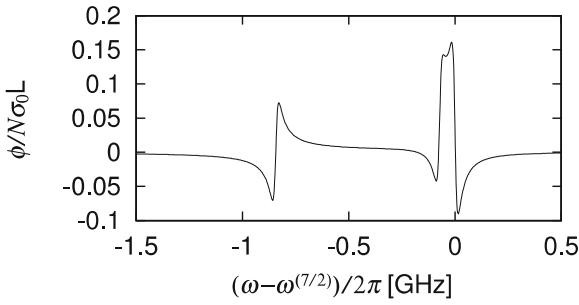
FIGURE 6 Rotation angle of spin-5/2 isotope. Here we used the value of the hyperfine splitting, $\omega^{(3/2)} - \omega^{(7/2)} = -2\pi \times 73$ MHz, and $\omega^{(5/2)} - \omega^{(7/2)} = -2\pi \times 844$ MHz [20], and we assumed the population is polarized at $m_I = +5/2$ state

FIGURE 7 Schematic of the optical pumping. The atom in $m_I \neq +I$ state absorb σ_+ light (*solid lines*), then emit $\sigma_\pm$ or π light (*dot lines*) and fall to a lower state. By repeating the absorptions and the emissions, all populations finally transfer to the $m_I = +I$ state

nally transfer to the $m_I = +I$ state. The details of the optical pumping are given in reference [18].

3   Experiments

For our experiments, we used the external cavity laser diode (ECLD) and injection-locking of a laser diode (LD) technique [21]. In Fig. 8, we show the basic setup to observe the paramagnetic Faraday rotation. The pump light is magnified with lenses so as to cover the atom distribution. For monitoring of the rotation angle, we constructed a polarimeter which consists of two photodiodes (PD) and a current sensitive amplifier.

Here, we note the property of the polarimeter. We define P_{in}, P_{out}, P_+ and P_- as the power in front of the atoms, behind the atoms, in front of the PD of the $+$ sense, and in front of the PD of the $-$ sense, respectively. The output of the polarimeter is proportional to $P_+ - P_- = P_{out} \sin(2\varphi)$. P_{out} can be measured by the relation $P_{out} = P_+ + P_-$. We also define the optical depth as $-\ln(P_{out}/P_{in})$. The optical depth for resonance is useful since it reflects $N\sigma_0 L$, which is the propor-

$M(F')$	Probability	$M(F')$	Probability
171(1/2)	1/3	173(7/2)	4/9
171(3/2)	2/3	173(3/2)	2/9
		173(5/2)	1/3

TABLE 2 Relative transition probabilities among the hyperfine sublevels for π polarized light

tional factor of the Faraday rotation as is shown in (7), (12), and (13). In the case of spin-nonzero isotopes, we must take into consideration the relative transition probabilities among the excited hyperfine states and the ground state to deduce $N\sigma_0 L$. In Table 2, we show the probability factors.

3.1   *Polarization spectroscopy with an atomic beam*

Firstly, we observed the paramagnetic Faraday rotation with an atomic beam. By use of an atomic beam, we could continuously observe the signal. The number density of the atomic beam was stable, and less insensitive for the photon scattering. By pumping with circularly polarized light of an appropriate frequency, we could isotope-selectively observe the paramagnetic Faraday rotation.

The atomic beam was generated from a metallic Yb sample in an atomic oven at about 500 °C. The oven was in a vacuum chamber at a pressure of 3×10^{-4} Pa. A Helmholtz coil was set around the atomic beam so as to cancel the stray magnetic field of about 1×10^{-4} T parallel to the probe light. In Fig. 9, we show the experimental apparatus set up.

In Fig. 10, we show the absorption spectrum with the probe light. It shows that the atomic beam was so well collimated that the linewidth caused by the transverse Doppler broadening is $\Gamma^* = 2\pi \times 57$ MHz, about twice that of the natural linewidth Γ, obtained from the fitting with the isotope shifts and the hyperfine splittings [20], and the relative transition probabilities for π polarized light among the hyperfine sublevels (Table 2). In the fitting, we approximated the Doppler broadening Γ^* as the natural line width Γ, known as the $T_2^* \to T_2$ approximation. From Fig. 10, we obtained $N\sigma_0 L = 0.18$ for ^{171}Yb and $N\sigma_0 L = 0.21$ for ^{173}Yb.

In Fig. 11, we show the Faraday rotation with the optical pumping. Simultaneously, we show the theoretical curves assuming the $T_2^* \to T_2$ approximations and the perfect polarization by the optical pumping. In Fig. 11a and b of the theoretical curve, we made corrections for the resonance frequency $\omega^{(3/2)}$ and $\omega^{(7/2)}$, respectively, for the imperfect linearity of the frequency sweep of our ECLD. As is shown in Fig. 11, the rotation angle, except for near resonance, agrees well with the theoretical estimation, which indicates that the optical pumping was ideally performed.
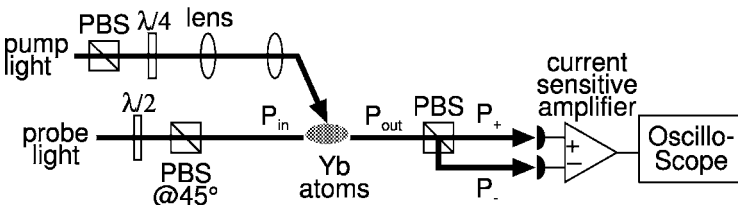
FIGURE 8 Basic setup of the system. The paramagnetic Faraday rotation appears after optical pumping with circularly polarized light. The rotation angle is monitored with a polarimeter. PBS: polarization beam splitter, $\lambda/4$: quarter-wave plate, $\lambda/2$: half-wave plate. P_{in}, P_{out}, P_+ and P_- are the power values at the each point
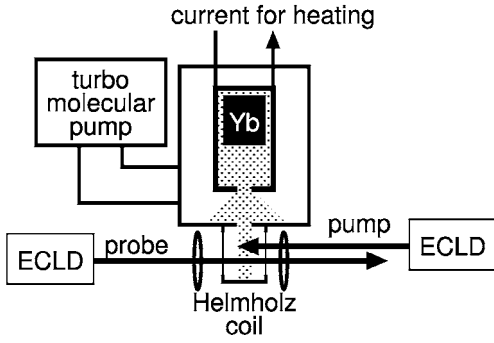
FIGURE 9 Atomic beam system and experimental setup for the polarization spectroscopy. The atomic oven was heated by electric current to obtain a high-temperature of 500 °C. The atomic beam was collimated by an aperture of diameter $L = 5$ mm, in a chamber evacuated by a turbo molecular pump. A Helmholtz coil was set around the atomic beam so as to cancel the stray magnetic field parallel to the probe light
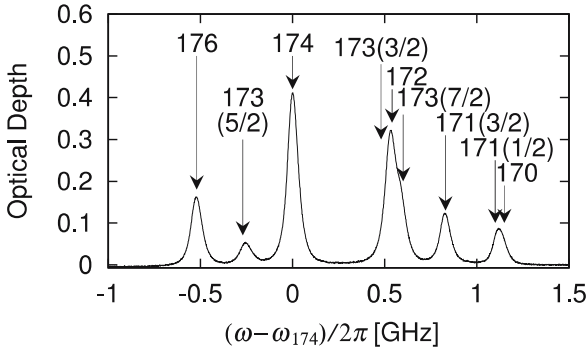

FIGURE 10 Absorption spectrum of the atomic beam. It shows that the atomic beam was so well collimated that the linewidth caused by the transverse Doppler broadening is $\Gamma^* = 2\pi \times 57$ MHz, about twice that of the natural linewidth Γ. ω_{174} is the resonance frequency of ^{174}Yb, which is the most naturally abundant isotope (31.8%). The numbers in the parentheses represent hyperfine quantum numbers

The rotation angles were small at some near-resonant frequencies compared with the theoretical values. We think that this is due to the depolarization by the probe light. The photon scattering rate of a two-level system can be written as [18]

$$r = \frac{\Gamma}{4} \frac{\Omega^2}{(\omega_0 - \omega)^2 + (\Gamma/2)^2 + (\Omega/2)^2} . \quad (14)$$

The transit time of the probe region for an atom T can be estimated as $T \sim 2w/v = 0.9$ μs, where w is the probe beam waist measured as $w = 0.14$ mm, and v is the squared-average longitudinal velocity of the atomic beam estimated as $v = 0.3$ km/s from the oven temperature. Since the intensity of the probe light at the atomic beam region was 0.55 mW/mm^2, the photon absorption rate at the peak of the dispersive function $\omega_0 - \omega = \Gamma^*/2$, becomes $r \sim 4 \times 10^7$ s^{-1}. Therefore, the scattering counts becomes $rT \sim 4 \times 10^1$, which is large enough to decrease the population differences. Strictly speaking, (14) is inappropriate for discussing the photon scattering rate at near-resonance, because ^{171}Yb and ^{173}Yb are not a two-level system. However, we emphasize that the rotation angle except for the near resonance agrees well with the theoretical estimation.

As (7) indicates, the stray magnetic field parallel to the probe light leads to diamagnetic Faraday rotation. In Fig. 11,
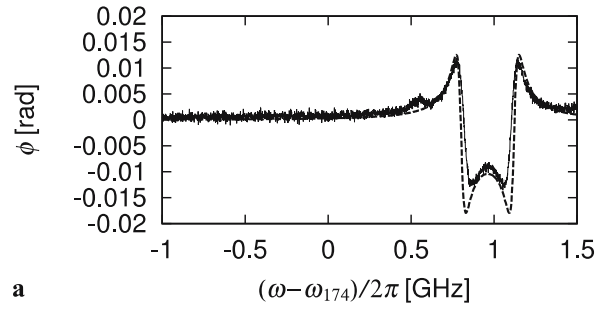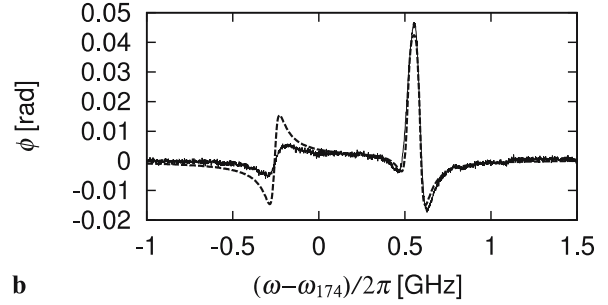
FIGURE 11 Results of the Faraday rotation (*solid lines*), and theoretical curves assuming perfect polarization (*dot lines*). (**a**) The frequency of the pumping light was tuned at 171(1/2) resonance. (**b**) The frequency of the pumping light was tuned at 173(5/2) resonance

the rotation angle vanished near the resonance frequencies of ^{170}Yb, ^{172}Yb, ^{174}Yb, and ^{176}Yb, which indicates that the stray magnetic fields were well suppressed by the Helmholtz coil, otherwise we could in fact observe the Faraday rotation as in Fig. 2b. We emphasize that the magnetic field is not necessary for spin polarization because the optical pumping process is faster than the Larmor precession. This is the reason why Yb can be easily highly polarized.

3.2 Ballistically expanding cold ^{171}Yb atoms released from MOT

Secondly, we observed the paramagnetic Faraday rotation of the ballistically expanding cold atoms released from MOT. By use of cold atoms, it became possible to probe an atomic ensemble for a long time, which was impossible for the atomic beam due to the longitudinal velocity.

In Fig. 12, we show the experimental setup. By using a glass cell ($50 \times 50 \times 100$ mm) at the MOT chamber, we could obtain good optical access to atoms in the MOT. The background gas pressure in the glass cell was about 5×10^{-6} Pa. The magnetic gradient created by the anti-Helmholz coil was 4.3×10^{-4} T/mm along the axis. In Fig. 13, we show the light source system. By using injection-lock techniques [21], the frequency stabilizations of the two LDs were experimentally simplified. In Fig. 14a, we show their frequencies. The frequency of the master ECLD was tuned at the red side of $\omega^{(3/2)}$, that of the slower light was at -216 MHz from $\omega^{(3/2)}$, that of MOT light was at -26 MHz from $\omega^{(3/2)}$, and that of the pumping light was close to $\omega^{(1/2)}$.

The temperature of the trapped atom was typically 4 mK estimated from the release and recapture method with an MOT beam diameter of 10 mm, and a release time of 7.5 ms. The trap lifetime was 0.3 s, measured by the decay of the fluorescence after switching off the slower beam. The diameter of
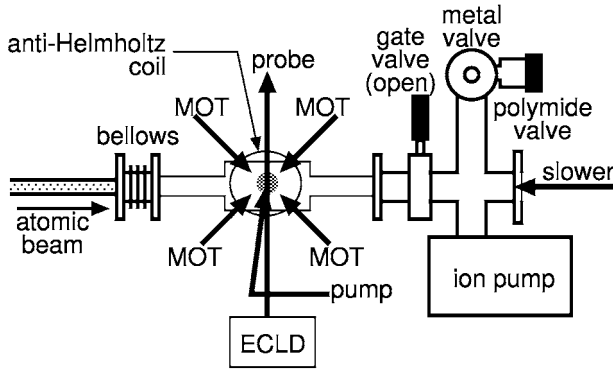
FIGURE 12 Experimental setup. By using a glass cell at the MOT chamber, we could obtain good optical access to atoms. The background gas pressure in the glass cell was about 5×10^{-6} Pa. The magnetic gradient created by the anti-Helmholz coil was 4.3×10^{-4} T/mm along the axis
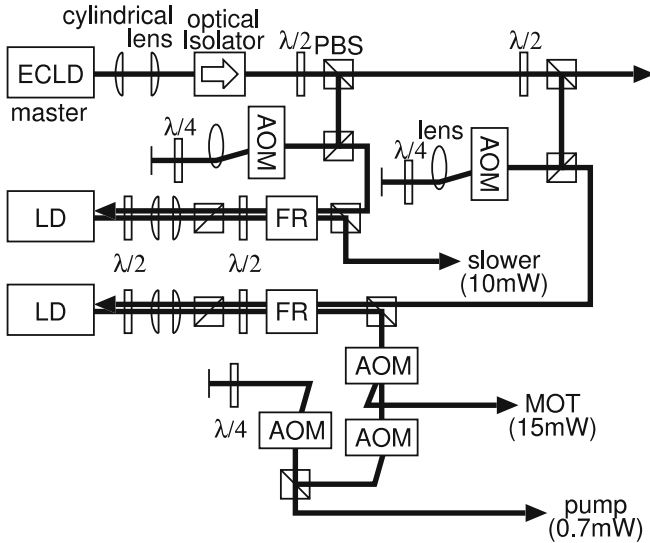

FIGURE 13 Schematic of the light source for the MOT and optical pumping of ^{171}Yb. FR:Faraday rotator, AOM:acousto-optic modulator. The typical powers are also shown

the trapped atom cloud was $L \sim 2$ mm, as roughly estimated by a CCD camera. The trapped atom number was typically estimated as 7×10^6 from the intensity of the fluorescence. It should be noted that we also succeeded in the MOT of ^{170}Yb, ^{174}Yb, and ^{176}Yb using the same system.

The optical depth before and after the release from the MOT is shown in Fig. 14b, which was measured by the transmission of the weak probe with an intensity of $0.06\,\mu$W/mm^2 at the resonant frequency $\omega^{(3/2)}$. This data can be fitted as an exponential function $d\exp(-t/\tau)$, where d and τ are free parameters, and t is the time of flight. As a result, $N\sigma_0 L$ in the probe region is estimated as $N\sigma_0 L = 3d/2 = 7.5 \times 10^{-2}$, and the decay time is estimated as $\tau = 2.2$ ms. The decay after the release was due to the expansion of the atom distribution. Since the beam waist of the probe light was $w = 0.5$ mm, the average velocity of the atom can be estimated as $v \sim w/\tau = 0.2$ m/s, which was three orders of magnitude smaller than the atomic beam.

With this setup, we polarized the atoms via optical pumping after the release from the MOT, while probing the Faraday rotation with an intensity of $0.3\,\mu$W/mm^2. The detuning of
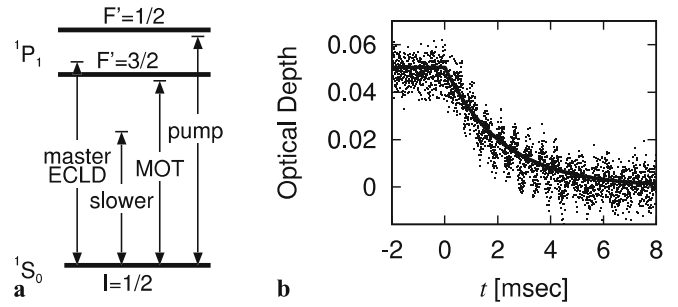
FIGURE 14 (a) Each frequency of light. The frequency of the master ECLD was tuned at the red side of $\omega^{(3/2)}$, that of the slower light was at -216 MHz from $\omega^{(3/2)}$, that of MOT light was at -26 MHz from $\omega^{(3/2)}$, and that of the pumping light was close to $\omega^{(1/2)}$. (b) The optical depth of the MOT measured by the probe light whose frequency was tuned at $\omega^{(3/2)}$. The *dot* is the experimental value, and the *line* is the fitting curve
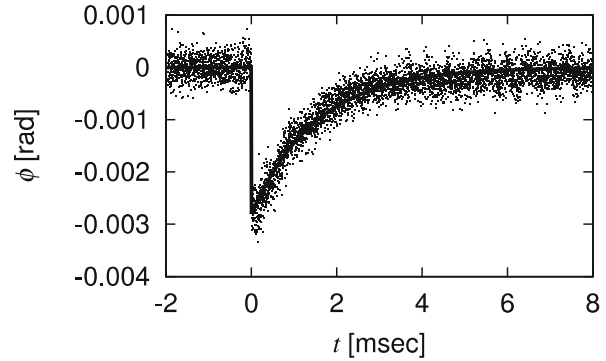
FIGURE 15 Experimental result of the rotation angle (*dot*). The rotation angle decays caused by the expansion of the atom distribution from the probe region. The *solid line* is the theoretical curve estimated from Fig. 14b

the probe beam was set at $\omega - \omega^{(3/2)} = 2\pi \times 0.16$ GHz, which corresponds to the center of the two hyperfine resonances (see Fig. 4 and also Fig. 11a). At this probe frequency, $\varphi/pN\sigma_0 L$ is 3.0×10^{-2}. In Fig. 15, we show the experimental result of the Faraday rotation and the fitting curve by an exponential function. The experimental result agrees well with the theoretical estimation assuming perfect polarization $p = 1$. It should be noted that the optical pumping was completed much more rapidly when compared with the expansion time.

The probed atom number was $2S = N\pi w^2 L = 7 \times 10^5$, which was one order of magnitude smaller than the trapped atom number. Therefore, the whole trapped atom could not be observed. To improve the matching between the atomic distribution and the probe region, compression of the MOT will be required.

3.3   *Larmor precession of trapped ^{171}Yb*

Finally, we observed the Faraday rotation signal of ^{171}Yb atoms trapped in a single FORT and its Larmor precession due to an applied magnetic field. By using FORT, the decay caused by the ballistic expansion was overcome.

In Fig. 16, we describe the experimental setup. As the FORT beam, we used a diode-pumped solid state (DPSS) laser. After the loading of the atom from the MOT to FORT, we polarized the atoms via the optical pumping. As a result, the trapped atom number was $2S = 8 \times 10^6$, the temperature was 0.1 mK, the distribution was the pencil shape of
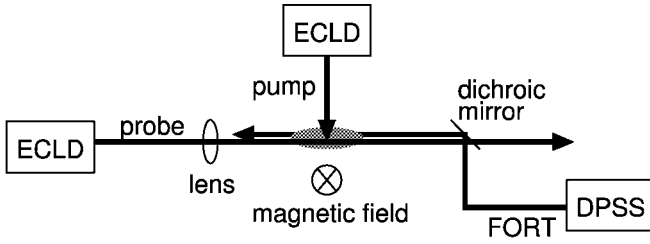
FIGURE 16 Experimental setup for the observation of the Larmor precession of trapped ^{171}Yb. After the optical pumping, the atom precessed by an applied magnetic field. The precession was monitored via the paramagnetic Faraday rotation of the probe light
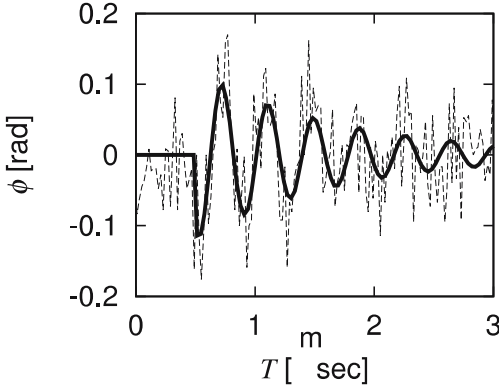

FIGURE 17 Experimental result of the rotation angle (*dot line*). The *bold line* is the fitting curve, based on (15). The rotation angle oscillates at the Larmor frequency, and decays by the trap loss of the atomic ensemble

the waist 3 μm, and the length $L = 1$ mm [16]. The probe beam of the diameter 30 mm was focused by a lens of focal length 300 mm, so as to match the atomic distribution. In spite of these efforts, the beam waist of the probe beam at the atom distribution was $w = 30$ μm, which was not narrow enough for atomic distribution. Therefore, effectively $N\sigma_0 L$ in the expression of φ becomes smaller and $N\sigma_0 L = 2S\sigma_0/(\pi w^2) = 2 \times 10^2$. The detuning of the probe beam was set at $\omega - \omega^{(3/2)} = 2\pi \times 1.6$ GHz, which was blue detuning so as not to induce photoassociation [22]. At this probe frequency, $\varphi/pN\sigma_0 L$ is 3.8×10^{-4}. Since the magnetic field was measured as 3.5×10^{-4} T, the precession frequency was $\omega_B = 2\pi \times 2.6$ kHz, derived from the gyromagnetic ratio 7.50×10^6 Hz/T.

In Fig. 17, we show the experimental result, where T is the time after the optical pumping. It should be noted that this signal represents the difference between the Faraday rotation signals with and without the optical pumping.

This signal can be fitted by

$$\varphi = \Phi \exp(-T/\tau) \sin(\omega_B T + \theta) \ , \tag{15}$$

where Φ, τ, and θ are free parameters. The frequency agrees with the Larmor frequency ω_B. The amplitude of the rotation angle Φ also agrees with the assumption of perfect polarization $p = \sin(\omega_B T + \theta)$.

We think the reason for the decay is that the photon scattering decreases $N\sigma_0 L$. Since the probe intensity at the atom was $I = 0.70$ mW/mm^2, the photon scattering rate becomes $r = 8.7 \times 10^3$ s^{-1}. The acceleration roughly becomes $a \sim \hbar\omega r/M_{171}c = 51$ m/s^2, where M_{171} is the mass of ^{171}Yb.

The hold time in the trap region roughly becomes $\sqrt{2L/a} = 6$ ms. This value is comparable to the experimental result. Another reason for the decay is the depolarization caused by the photon scattering. The trap loss and the depolarization can be suppressed by taking more off-resonance and reducing the intensity. Moreover, by improving the probe light beam diameter so as to match the atom distribution, the rotation angle remains large enough as is calculated in [23].

4   Conclusions

In this paper, we derive the theoretical value of the paramagnetic Faraday rotation of Yb atoms, and report its observation. As the atomic samples, we used an atomic beam, released atoms from a MOT, and trapped atoms in a FORT. By use of an atomic beam which includes many isotopes, we demonstrated the polarization spectroscopy by isotope-selective optical pumping. Using released atoms from the MOT, we observed the Faraday rotation of the ballistically expanding cold atoms. By use of the trapped atom in FORT, we observed the Larmor precession by an applied magnetic field. In this system, we have succeeded in almost perfect polarization, which was evaluated from the rotation angle. These results are important progresses for the realization of spin QND, spin squeezing via one-axis twisting with coherent light [23], the search for the permanent electric dipole moment of ytterbium atom [11], and so on.

REFERENCES

1 D. Budker, W. Gawlik, D.F. Kimball, S.M. Rochester, V.V. Yashchuk, A. Weis, Rev. Mod. Phys. **74**, 1153 (2002)
2 W. Happer, Rev. Mod. Phys. **44**, 169 (1972)
3 Y. Takahashi, K. Honda, N. Tanaka, K. Toyoda, K. Ishikawa, T. Yabuzaki, Phys. Rev. A **60**, 4974 (1999)
4 A. Kuzmich, L. Mandel, J. Janis, Y.E. Young, R. Ejnisman, N.P. Bigelow, Europhys. Lett. **42**, 481 (1998)
5 A. Kuzmich, L. Mandel, J. Janis, Y.E. Young, R. Ejnisman, N.P. Bigelow, Phys. Rev. A **60**, 2346 (1999)
6 A. Kuzmich, L. Mandel, N.P. Bigelow, Phys. Rev. Lett. **85**, 1594 (2000)
7 B. Julsgaard, A. Kozhekin, E.S. Polzik, Nature (London) **413**, 400 (2001)
8 J.M. Geremia, J.K. Stockton, H. Mabuchi, Science **304**, 270 (2004)
9 B. Julsgarrd, J. Sherson, J.I. Cirac, J. Flurášek, E.S. Polzik, Nature (London) **432**, 482 (2004)
10 H. Terashima, M. Ueda, quant-ph/0507020
11 Y. Takahashi, M. Fujimoto, T. Yabuzaki, A.D. Singh, M.K. Samal, B.P. Das, in *Proceedings of CP Violation and its Origins*, ed. by K. Hagiwara (KEK Reports, Tsukuba 1997)
12 T. Isayama, Y. Takahashi, N. Tanaka, K. Toyoda, K. Ishikawa, T. Yabuzaki, Phys. Rev. A **59**, 4836 (1999)
13 K. Honda, Y. Takahashi, T. Kuwamoto, M. Fujimoto, K. Toyoda, K. Ishikawa, Y. Yabuzaki, Phys. Rev. A **59**, R934 (1999)
14 T. Kuwamoto, K. Honda, Y. Takahashi, T. Yabuzaki, Phys. Rev. A **60**, R745 (1999)
15 K. Honda, Y. Takasu, T. Kuwamoto, M. Kumakura, Y. Takahashi, T. Yabuzaki, Phys. Rev. A **66**, 021401(R) (2002)

16 Y. Takasu, K. Honda, K. Komori, M. Kumakura, Y. Takahashi, T. Yabuzaki, Phys. Rev. Lett. **90**, 023 003 (2003)
17 H.J. Metcalf, P. van der Straten, *Laser Cooling and Trapping* (Springer, Tokyo, 1999)
18 D. Suter, *The Physics of Laser-Atom Interactions* (University Press, Cambridge, 1997)
19 J.J. Sakurai, *Modern Quantum Mechanics* (Addison-Wesley, Tokyo, 1995)
20 A. Banerjee, U.D. Rapol, D. Das, A. Krishna, V. Natarajan, Europhys. Lett. **63**, 340 (2003)
21 K. Komori, Y. Takasu, M. Kumakura, Y. Takahashi, T. Yabuzaki, Jpn. J. Appl. Phys. **42**, 5059 (2003)
22 Y. Takasu, K. Komori, K. Honda, M. Kumakura, T. Yabuzaki, Y. Takahashi, Phys. Rev. Lett. **93**, 123 202 (2004)
23 M. Takeuchi, S. Ichihara, T. Takano, M. Kumakura, T. Yabuzaki, Y. Takahashi, Phys. Rev. Lett. **94**, 023 003 (2005)